1 Perturbative Stability of Massless Scalars in AdS_4

Will be published to the arXiv, then submitted to JHEP

1.1 Contributions

What my contributions were

Paper Title

To Appear on arxiv.org

Brad Cownden[1], Nils Deppe[2], and Andrew R. Frey[3,4]

[1]*Department of Physics & Astronomy,*
University of Manitoba
Winnipeg, Manitoba R3T 2N2, Canada
cowndenb@myumanitoba.ca

[2]*Cornell Center for Astrophysics and Planetary Science and Department of Physics,*
Cornell University
122 Sciences Drive, Ithaca, New York 14853, USA
nd357@cornell.edu

[3]*Department of Physics & Astronomy,*
University of Manitoba
Winnipeg, Manitoba R3T 2N2, Canada
[4]*Department of Physics and Winnipeg Institute for Theoretical Physics,*
University of Winnipeg
515 Portage Avenue, Winnipeg, Manitoba R3B 2E9, Canada
a.frey@uwinnipeg.ca

We construct a family of perturbative solutions for massless scalar fields in AdS_4 using the *Two-Time Formalism* (TTF) to high eigenmode numbers. We furthermore investigate the validity of *quasi-periodic* (QP) solutions with high j_{max} values and examine their stability to perturbations. Finally, check that TTF and QP solutions continue to satisfy the Einstein equation at times greater than $t \sim \epsilon^{-2}$ and compare these results to the full numerical solutions at low amplitude.

1.2 Introduction

The question of the nonperturbative stability of AdS_{d+1} has been examined extensively, both as a question of mathematical physics and given its application to the AdS/CFT correspondence; see [?] for a recent review. Beginning with the seminal work of [?], many works [?, ?, ?, ?, ?] have demonstrated the generic instability of AdS_{d+1} gravity minimally coupled to a scalar field in a variety of dimensions. The primary driver of the instability in the fully nonlinear system is the weakly turbulent flow of energy to short length scales; in the perturbative description, secular growth of resonant terms with high frequencies triggers the collapse [?,?,?]. However, [?,?,?] (and others) have shown that some initial conditions in asymptotically AdS spacetime resist gravitational collapse and therefore form islands of stability in the space of initial data. The stable solutions within the island are variously known as oscillons or breathers for real scalars [?, ?, ?, ?], boson stars for complex scalars [?, ?], and geons for pure gravity [?, ?].[1] [?, ?, ?] have shown that the classification of initial

[1]citations given for studies in asymptotically AdS space.

data is more complex nonperturbatively, intriguingly finding evidence of chaos at the boundary between stable and unstable initial data. While past studies have mostly dealt with spherically symmetric collapse, an increasing amount of work is focused on removing this restriction [?, ?, ?].

While the nonperturbative physics of AdS instability requires numerical study, a perturbative formulation should give insight into stability at low amplitudes. In a naive perturbation theory, the fully resonant spectrum of eigenmodes of pure AdS leads to secular growth; this can be removed order by order by frequency shifts if the initial data consists of a single eigenmode but not for superpositions of eigenmodes [?]. If instead the amplitude and phase of each eigenmode are allowed to flow slowly, resummation of the perturbation theory leads to a ladder of coupled first-order ordindary differential equations describing the flow. There are several equivalent methods to arrive at the flow equations: a "two-time formalism" (similar to a temporal gradient expansion for the amplitude and phase variables) [?], a renormalization-like formalism [?, ?], time averaging [?, ?], and keeping only resonant source terms [?]. (We will commonly refer to the perturbative theory as the TTF theory, for two-time formalism.) A key feature of this perturbative theory is a scaling symmetry $\phi(t) \to \epsilon^{-1}\phi(\epsilon^2 t)$, so it is possible to divide out the amplitude of the scalar and describe the solution in terms of the "slow time" $\tau = \epsilon^2 t$. Furthermore, the perturbative theory has conserved quantities beyond the total energy E, including a "particle number" N, which leads to inverse cascades in energy from higher eigenmodes to lower modes along with the expected direct cascades from low to high. On the other hand, while the flow equations are significantly less computationally intensive than the full Einstein and Klein-Gordon equations, finding a solution requires truncating to a maximum eigenmode number j_{max}.

At a given mode truncation j_{max}, the TTF theory has stable quasi-periodic (QP) solutions with constant energy spectrum as described in [?, ?], and other stable solutions orbit the QP solutions in phase space. Since the amplitude scales out of the TTF, the QP solutions are described by "temperature" $T = E/N$; for fixed maximum mode number j_{max}, the maximum possible temperature is $d + 2j_{max}$. The QP solutions are special in that the time-dependence of each mode is harmonic, so QP solutions satisfy algebraic equations; [?] found low-temperature solutions to these equations directly. To reach higher temperatures, [?] perturbed low-temperature solutions by the addition of energy. Our main concern in this work is the persistence of QP solutions, especially those at high temperatures, as j_{max} increases since the full TTF theory takes $j_{max} \to \infty$.

**** LEFT THE REST ALONE, NEED TO DISCUSS ORGANIZATION AND METHODS WHEN WE'RE FINISHED

We show that high temperature QP solutions are very sensitive to truncation error and cannot be interpreted as physically relevant solutions. We then examine the time evolution of large j_{max} QP solutions at all temperatures in both the perturbative theory and the full, nonlinear theory. **[OTHER MAJOR GOALS HERE]**

This work is organized as follows: we begin in § 1.3 with a review of the linearized solutions for a minimally coupled, massless scalar field in AdS_{d+1} and establish the renormalization flow equations that govern the time evolution of the amplitude and phase functions in the scalar field. In § 1.4, we find quasi-periodic solutions in AdS_4 by directly solving a set of algebraic equations, and discuss the viability of reaching new QP solutions through repeated application of a perturbative scheme. We then examine the time evolution of a wide range of QP solutions in § 1.5 in both the linearized theory and the full, nonlinear system. We end with a discussion in § 1.6.

1.3 Minimally Coupled Scalar Fields in AdS$_{d+1}$

Consider a spherically-symmetric, asymptotically AdS$_{d+1}$ spacetime with characteristic curvature ℓ. Written in Schwarzschild-like coordinates, the metric in units of AdS scale is given by

$$ds^2 = \frac{1}{\cos^2(x)}\left(-Ae^{-2\delta}dt^2 + A^{-1}dx^2 + \sin^2(x)d\Omega^{d-1}\right), \tag{1.1}$$

where the radius $x \in [0, \pi/2]$ and $-\infty < t < \infty$. A minimally-coupled, massless scalar field $\phi(t, x)$ is subject to the following Einstein and Klein-Gordon equations:

$$G_{ab} + \Lambda g_{ab} = 8\pi\left(\nabla_a\phi\nabla_b\phi - \frac{1}{2}g_{ab}(\nabla\phi)^2\right) \tag{1.2}$$

$$0 = \frac{1}{\sqrt{-g}}\partial_a\sqrt{-g}\, g^{ab}\partial_b\phi\,. \tag{1.3}$$

The canonical equations of motion for the scalar field are

$$\partial_t\phi = Ae^{-\delta}\Pi, \quad \partial_t\Phi = \partial_x(Ae^{-\delta}\Pi), \quad \text{and} \quad \partial_t\Pi = \frac{\partial_x\left(\Phi Ae^{-\delta}\tan^{d-1}(x)\right)}{\tan^{d-1}(x)}, \tag{1.4}$$

where the canonical momentum is $\Pi(t, x) = A^{-1}e^{\delta}\phi$ and $\Phi(t, x) \equiv \partial_x\phi$ is an auxiliary variable. In terms of these fields, (1.2)-(1.3) reduce to

$$\partial_x\delta = -\left(\Pi^2 + \Phi^2\right)\sin(x)\cos(x), \tag{1.5}$$

$$\partial_x A = \frac{d - 2 + 2\sin^2(x)}{\sin(x)\cos(x)}(1 - A) - A\sin(x)\cos(x)(\Pi^2 + \Phi^2)\,. \tag{1.6}$$

1.3.1 Linearized Solutions

The linearized scalar field solutions come from expanding in terms of a small amplitude

$$\phi(t, x) = \sum_{j=0}^{\infty}\epsilon^{2j+1}\phi_{2j+1}(t, x), \quad A(t, x) = 1 - \sum_{j=1}^{\infty}\epsilon^{2j}A_{2j}(t, x), \quad \delta(t, x) = \sum_{j=1}^{\infty}\epsilon^{2j}\delta_{2j}(t, x). \tag{1.7}$$

Under this expansion, the $\mathcal{O}(\epsilon)$ terms give the linearized equation of motion for the scalar field:

$$\partial_t^2\phi_1 + \hat{L}\phi_1 = 0 \quad \text{where} \quad \hat{L}_1 \equiv -\frac{1}{\tan^{d-1}(x)}\partial_x\left(\tan^{d-1}(x)\partial_x\right). \tag{1.8}$$

The eigenvalues of $\hat{L}$ are simply $\omega_j^2 = (d + 2j)^2$ and the eigenfunctions are

$$e_j(x) = k_j\cos^d(x)P_j^{(\frac{d}{2}-1,\frac{d}{2})}(\cos(2x)) \quad \text{with} \quad k_j = \frac{2\sqrt{j!(j + d - 1)!}}{\Gamma(j + \frac{d}{2})}. \tag{1.9}$$

Note the the normalizations are chosen such that $\hat{L}e_j = \omega_j^2 e_j$ and

$$\langle e_i | e_j \rangle \equiv \int_0^{\frac{\pi}{2}} dx\, \bar{e}_i e_j \tan^{d-1}(x)\,. \tag{1.10}$$

By expanding the scalar field functions in terms of the eigenbasis given in (1.9) and substituting into (1.8), we find that the time-dependent functions $c_n^{(2j+1)}(t) = \langle \phi_{2j+1}(t,x), e_n(x) \rangle$ satisfy $\ddot{c}_j^{(1)} + \omega_j^2 c_j^{(1)} = 0$. The general solution for the scalar field is can then be written in terms of time-dependent amplitude and phase variables:

$$\phi_1(t,x) = \sum_{j=0}^{\infty} A_j(t) \cos\left(\omega_j t + B_j(t)\right) e_j(x)\,. \tag{1.11}$$

As discussed in [?, ?, ?], the integer nature of the mode frequencies mean that the spectrum is fully resonant. Unlike solutions such as oscillons, the resonant terms cannot be absorbed by a frequency shift and therefore result in *secular* terms: resonant contributions that grow rapidly with time and induce collapse. These resonant terms appear at $\mathcal{O}(\epsilon^3)$ and can be expressed in terms of a source, $S(t)$:

$$\ddot{\phi}_3 + \hat{L}\phi_3 = S \equiv 2(A_2 - \delta_2)\ddot{\phi}_1 + (\dot{A}_2 - \dot{\delta}_2)\dot{\phi}_1 + (A_2' - \delta_2')\phi_1'\,, \tag{1.12}$$

where A_2, δ_2 are the leading-order contributions to the metric functions in (1.7) that are determined by the $\mathcal{O}(\epsilon^2)$ backreaction with the metric. Projecting onto the $e_j(x)$ basis, the source term (*i.e.*, resonant contributions) can be expressed in terms of the time-dependent coefficients

$$\ddot{c}_j^{(3)} + \omega_j^2 c_j^{(3)} = S_j\,. \tag{1.13}$$

To control the growth of secular terms, [?] used resummation techniques to absorb singular contributions into the amplitude A_j and phase B_j of (1.11). This also resulted in a set of conserved quantities: the energy of the system, E, and particle number, N. The simulataneous conservation of both E and N implied that weakly turbulent systems exhibit dual cascades of energy, providing a mechanism through which two-mode data could remain stable [?].

1.3.2 Two-Time Formalism

The Two-Time Formalism (TTF) describes the solution to (1.8) in terms of slowly-modulating amplitude and phase variables, A_j and B_j, that are functions of the slow time $\tau = \epsilon^2 t$,

$$\phi(t,x) = \epsilon \sum_{j=0}^{\infty} A_j(\epsilon^2 t) \cos\left(\omega_j t + B_j(\epsilon^2 t)\right) e_j(x). \tag{1.14}$$

The next non-trivial order in the equations of motion include gravitational self-interactions of the scalar field, and provides source terms for A_j and B_j. Following the time-averaging procedure of [?]

– and using the resonance condition $\omega_i + \omega_j = \omega_k + \omega_l$ to eliminate one of the indices – the l^{th} amplitude and phase are given by

$$-\frac{2\omega_l}{\epsilon^2}\frac{dA_l}{dt} = \sum_{i\neq l}^{l\leq i+j}\sum_{j\neq l} S_{ij(i+j-l)l} A_i A_j A_{i+j-l} \sin\left(B_l + B_{i+j-l} - B_i - B_j\right), \tag{1.15}$$

$$\begin{aligned}-\frac{2\omega_l A_l}{\epsilon^2}\frac{dB_l}{dt} &= T_l A_l^3 + \sum_{i\neq l} R_{il} A_i^2 A_l \\ &\quad + \sum_{i\neq l}^{l\leq i+j}\sum_{j\neq l} S_{ij(i+j-l)l} A_i A_j A_{i+j-l} \cos\left(B_l + B_{i+j-l} - B_i - B_j\right) .\end{aligned} \tag{1.16}$$

The coefficients T, R, S are calculated directly from integrals over the product of eigenmodes and contain some useful symmetry properties: the integrals vanish except with the resonance condition $\omega_i + \omega_j = \omega_l$ is met.

Computationally, we find it more convenient to write T, R, S in terms of auxiliary coefficients with greater symmetry properties (as shown in [**?**]). The explicit expressions for these integrals in the interior gauge, in which $\delta(t, x = 0) = 0$, are given in appendix B.

Using a complex amplitude of the form $\mathcal{A}_j(\tau) = A_j \exp(-iB_j)$ in (1.14) allows us to combine equations (1.15) and (1.16) into a single TTF equation:

$$-2i\omega_l \frac{\mathcal{A}_l}{d\tau} = T_l|\mathcal{A}_l|^2\mathcal{A}_l + \sum_{i\neq l} R_{il}|\mathcal{A}_i|^2\mathcal{A}_l + \sum_{i\neq l}^{l\leq i+j}\sum_{j\neq l} S_{ij(i+j-l)l}\mathcal{A}_i\mathcal{A}_j\bar{\mathcal{A}}_{i+j-l} . \tag{1.17}$$

1.4 Quasi-periodic Solutions in AdS_4

The stability of the solutions to (1.17) can be examined using a *quasi-periodic* (QP) ansatz for the complex amplitude,

$$\mathcal{A}_j = \alpha_j e^{i\beta_j \tau} , \tag{1.18}$$

where $\alpha_j, \beta_j \in \mathbb{R}$. Substituting (1.18) into (1.14) allows us to relate the QP modes α_j and β_j to the amplitude/phase modes via $A_j = 2\alpha_j$, $B_j = \beta_j \tau$. When we examine how well the QP solutions solve the Einstein equations, we use this conversion to re-construct the scalar and metric fields from the QP solutions. The time dependence in (1.17) is removed via the condition $\beta_j = \beta_0 + j(\beta_1 - \beta_0)$, leaving β_0 and β_1 as unknown parameters. Considering modes of (1.14) up to some j_{max}, the QP ansatz results in a set of $j_{max} + 1$ algebraic equations for $j_{max} + 3$ unknowns

$$2\omega_l\alpha_l\beta_l = T_l\alpha_l^3 + \sum_{i\neq l} R_{il}\alpha_i^2\alpha_l + \sum_{i\neq l}^{l\leq i+j}\sum_{j\neq l} S_{ij(i+j-l)l}\alpha_i\alpha_j\alpha_{i+j-l} . \tag{1.19}$$

As shown in [**?**, **?**], the TTF is invariant under a $U(1)$ transformation that leads to the conserved quantities

$$E = 4\sum_j \omega_j^2\alpha_j^2 \qquad \text{and} \qquad N = 4\sum_j \omega_j\alpha_j^2 . \tag{1.20}$$

These definitions allow for two of the free parameters to be fixed. Families of solutions can be examined by fixing $\alpha_0 = 1$ and sampling a range of α_1 values in the range $\alpha_1 \ll \alpha_0$. The families of solutions can be distinguished by their "temperature", or energy per particle number $T = E/N$.

Practically speaking, finding solutions to the j_{max} equations that arise from (1.17) requires truncating the series at a finite value $j_{max} < \infty$. These solutions must continue to be present and unaffected by increasing j_{max} to represent true solutions to the perturbative system.

1.4.1 Persistence at Large j_{max}

The question of edge effects in determining the stability of a particular solution is important to investigate. For instance, if a particular solution to (1.19) is found for some α_1 when $j_{max} = 50$, does this continue to be a solution when we consider more modes, say $j_{max} = 250$? By following the methods outlined in appendix A, we are able to start with a low j_{max} solution and incrementally increase the number of modes being considered up to several hundred. This method was found to be more successful, given the optimization algorithms being used, than other seeding methods.

As an example, consider solutions to (1.19) with the conditions $\alpha_0 = 1.0$ (since all QP solutions are defined up to an overall scale, $\alpha_0 = 1.0$ is taken to always be true) and $\alpha_1 = 0.2$, which corresponds to an initial temperature of $T_0 \simeq 3.146$. In figure 1.1a, we present an overlay of QP solutions generated by successive solving, fitting, and seeding from $j_{max} = 50$ to $j_{max} = 500$ for two families of QP solutions. Similar high j_{max} solutions were confirmed for $\alpha_1 \leq 0.442$.

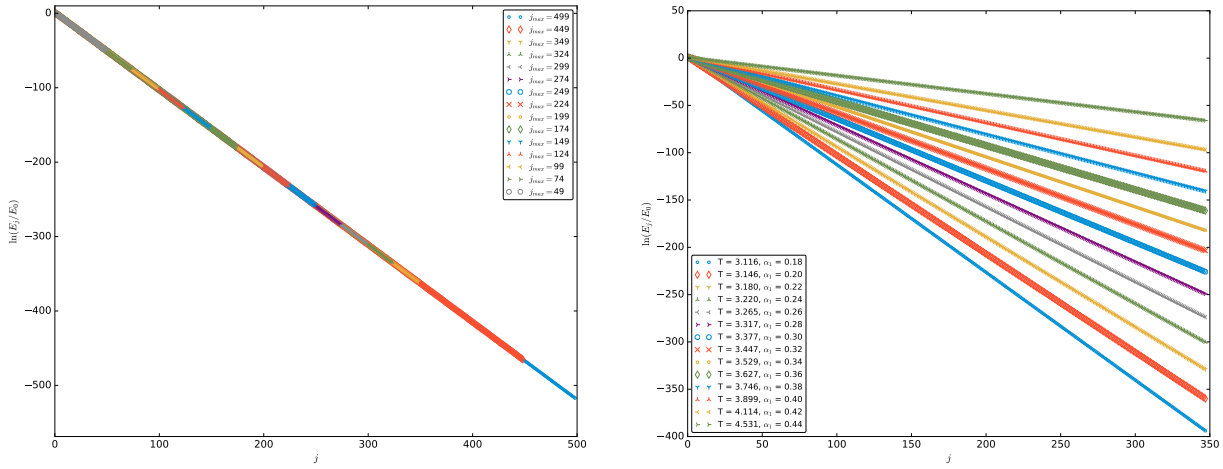

(a) *An overlay of QP solutions with* $\alpha_1 = 0.2$*, corresponding to* $T_0 \simeq 3.146$.

(b) *QP solutions up to* $j_{max} = 350$.

Figure 1.1: *Energy spectra for various QP solutions.*

When examining the range of α_1 values that result in QP solutions existing, it was found that any solution that existed at small j_{max} could be extended to large j_{max} with proper seeding and sufficient computing power. However, a hard limit exists at the maximum α_1 value of $\alpha_1 = 0.442$, corresponding to a temperature of $T \simeq 4.643$. Above this limit, no QP solutions can be found even for j_{max} values as low as $j_{max} = 50$. There seem to be no solutions that exist at low j_{max} that cease

to exist at high j_{max}. Furthermore, there is no corresponding lower limit to α_1 values; as $\alpha_1 \to 0$ with $\alpha_j > \alpha_{j+1}$, the TTF solution approaches the well-known single-mode solution.

1.4.2 High Temperature Perturbations

In [**?**], additional QP solutions can be found by repeatedly perturbing existing solutions. The addition of some energy δE corresponds to the changes $\alpha_j \to \alpha_j + u_j$ and $\beta_j \to \beta_j + \theta_1 + \omega_j\theta_2$. The perturbed quantities are given by the system of *linear* equations

$$\delta E = 4\sum_j \omega_j^2 \alpha_j u_j \tag{1.21}$$

$$\delta N = 4\sum_j \omega_j \alpha_j u_j = 0 \tag{1.22}$$

$$\begin{aligned} 0 = {} & \omega_l\left(\alpha_l(\theta_1 + \omega_l\theta_2) + \beta_l u_l\right) + 6T_l\alpha_l^2 u_l + 2\sum_{i\neq l} R_{il}(\alpha_i^2 u_l + 2\alpha_i\alpha_l u_l) \\ & + 2\sum_{i\neq l}^{l\leq i+j}\sum_{j\neq l} S_{ij(i+j-l)l}\left[u_i\alpha_j\alpha_{i+j-l} + u_j\alpha_i\alpha_{i+j-l} + \alpha_i\alpha_j u_{i+j-l}\right]. \end{aligned} \tag{1.23}$$

Therefore, by solving (1.21)-(1.23) for $\{u_j, \theta_1, \theta_2\}$, the existing QP solution can be updated and the process can be repeated.

For a standard QP solution with $\alpha_1 = 0.2$, the initial temperature is $T_0 = 3.146$. By applying the high temperature perturbation method described above, we are able to increase the temperature of the solution. However, this process must be examined with some scrutiny; applying repeated perturbations to a known solution does not guarantee the final result remains a valid solution. To investigate this further, we have implemented a solver that projects back down to the QP solution plane after either a set number of perturbations, or after every perturbation. When a solution can no longer be projected back to the QP plane, we have perturbed too far and the state no longer represents a quasi-periodic TTF solution.

Consider figure 1.2. When the result of the linear perturbations is projected back down to the QP plane every 5 iterations, we see that the solution approaches an attractor and is unable to accumulate enough energy to escape this local minimum before being projected back down to the QP plane. However, when the projection frequency is decreased to every 20 iterations, the attractor solution is able to be bypassed; note that as the iteration number increases, we actually see a *decrease* in α_1 value while the temperature continues to increase. At iteration 150 in figure 1.2b, there is a cusp in α_1 and a corresponding drop in temperature. Moreover, α_1 becomes negative after several hundred iterations.

Let us examine the energy spectra of the solutions shown in figure 1.3a. When projecting back to the QP plane every 5 perturbations, the energy spectra do not deviate far from the initial solution; however, no temperature increase is observed. We denote solutions found by this method as "threshold temperature" solutions. The threshold temperature T_{th} is robust against increases in j_{max} and therefore is independent of edge effects. See table 1.1 for further details.

When the projection frequency is decreased to 20 iterations an increase in temperature can be observed, as seen in figure 1.3b. However, the discontinuous behaviour of the temperature as a

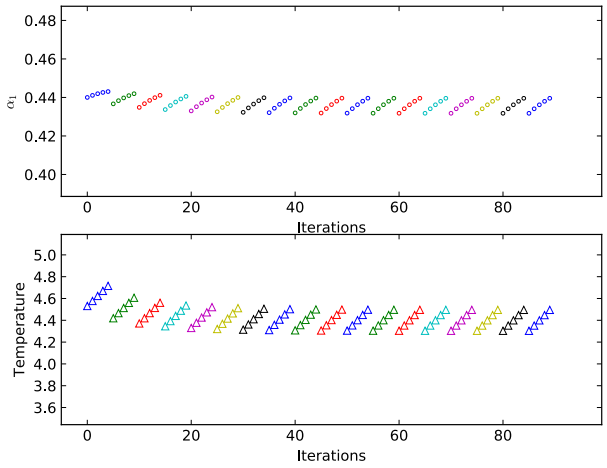

(a) *The result of applying repeated iterations of the linear perturbations to the initial QP solution of* $\alpha_1 = 0.44$*, projecting back to the QP plane every five iterations. The perturbation amount (*δE *in* (1.21)*) is fixed to* 1% *of the initial energy.*

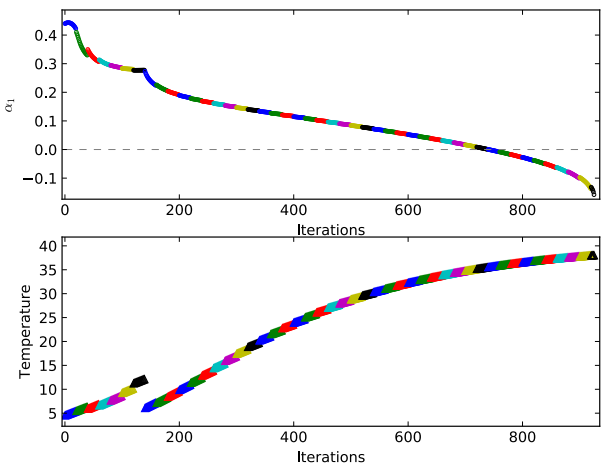

(b) *Starting from the same* $\alpha_1 = 0.44$ *QP solution, linear perturbations are again applied, this time projecting back to the QP plane every 20 iterations.*

Figure 1.2: *The results of projecting a* $j_{max} = 50$*,* $\alpha_1 = 0.44$ *solution back to the QP plane at various frequencies during high temperature perturbations. Colour changes indicate that the non-linear solver has been applied.*

function of iteration is a signal of the energy spectrum loosing its smooth profile (*c.f.* spectra of iterations 120 and 180). This in itself is not necessarily a breakdown of the quasi-periodic nature of the solution. Upon examining the condition number of the matrix formed by (1.21)-(1.23), we find that in fact the problem becomes ill-conditioned. This results in a absolute value of u_i that is greater than α_i; that is, the perturbative condition required to derive the system of linear equations (1.21)-(1.23) breaks down. For many prospective high-temperature solutions, this break-down of the perturbative condition is signalled by the development of spikes in the energy spectra caused by the values of α_j becoming negative. In § 1.5.2 we will examine the effects of using such solutions as initial data in the evolution of the QP solution.

1.4.3 Building High-Temperature Solutions

Despite high-temperature solutions being inaccessible via repeated energy perturbations, we may ask if such solutions can be found by using different methods. First, we consider perturbing a known QP solution to a high temperature *without* regular projections back to the QP plane. Then, at some sufficiently high temperature T_{max}, we attempt to project back to the QP plane. In figure 1.4a, the spectra of QP solutions before and after projection are shown for increasing j_{max}. For solutions with $j_{max} \geq 100$, high-temperature solutions are in fact projected to low-temperature solutions that may contain negative α_j values. Low-j_{max} solutions, however, appear to remain at high-temperatures after projecting back to the plane. We use this type of solution in our next method.

Starting with a low-j_{max}, high-temperature solution, we can use a fitting procedure similar to that

j_{max}	T_{th}	Iterations
50	4.30344575697724e+00	350
75	4.30344544264076e+00	210
100	4.30344544023857e+00	540
150	4.30344544024198e+00	280
200	4.30344544023915e+00	300

Table 1.1: *Values of the threshold temperature T_{th} for QP solutions with given j_{max}. Also included is the number of iterations applied (projecting back to the solution plane after every five iterations).*

used to find high-j_{max}, quasi-periodic solutions in § 1.4.1. Instead of fitting α_j values away from the highest modes, we instead apply the tail fitting the final 5 modes and use the fit to generate seed values for a $j_{max}+5$ solution. We see in figure 1.4b that this method results in spectra where energy becomes increasingly concentrated in high-j modes. In fact, for solutions with $j_{max} \geq 90$, and equal or greater amount of energy resides in the high-j modes than in the zero-mode. Intuitively, such a solution would collapse very quickly in the full system due to the high concentration of energy on small length scales. However, because we have arrived at this solution through the two-time formalism, evolution using (1.15)-(1.16) would ensure the solutions remain stable. To help quantify the stability of QP solutions against collapse, we calculate the scalar curvature at the origin.

1.4.4 Stability of QP Solutions

The Ricci Scalar at the Origin

While the TTF theory itself is stable by construction, we can examine the behaviour of the Ricci scalar at the origin for indications that collapse might occur in the full, nonlinear system. Large values or rapid increases in the Ricci curvature at the origin often indicates impending collapse **(ref?)** in numerical simulations. Therefore, we use increases in scalar curvature as a potential indication of collapse. In figure 1.5, we show the highly oscillatory behaviour of the Ricci scalar corresponding to the $T \simeq 66.6$ high-temperature solution presented in figure 1.4b. Note that the upper envelope of Π^2 is $\mathcal{O}(10^{12})$ immediately; this suggests that the high-temperature solution is *not stable* against collapse, even on perturbative timescales. Conversely, the constant behaviour and maximum amplitude $\mathcal{O}(10^4)$ of Π^2 for the $T \simeq 3.15$ QP solution – over multiples of the perturbative timescale – confirms that the solution remains quasi-periodic and does not collapse.

Constraint Equations

Another indicator of possible collapse and/or violation of the perturbative approximation is the growth of residuals when the TTF solutions are substituted into the Einstein equations. The residuals are calculated by reconstructing the time dependence of the scalar field and its derivatives using the amplitude-phase variables, and comparing the $\mathcal{O}(\epsilon^2)$ values of the derivatives of the metric

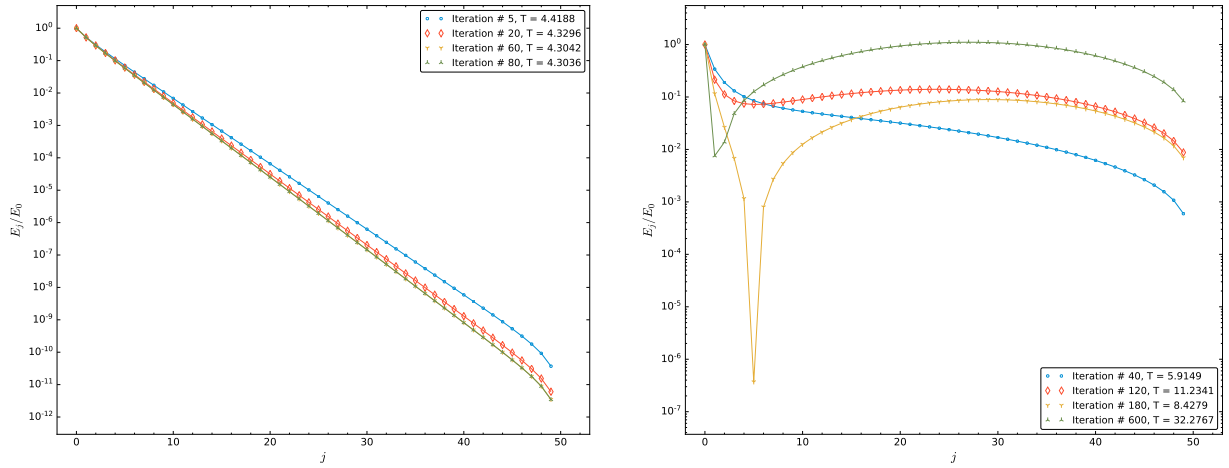

(a) *Energy spectra when projecting back to the QP solution plane every 5 iterations for an initial $\alpha_1 = 0.44$, QP solution (see figure 1.2a for temperature and α_1 as a function of iteration).*

(b) *The same initial QP solution as figure 1.3a is used, but is projected back to the QP plane every 20 iterations.*

Figure 1.3: *Comparing energy spectra of high-temperature perturbations of an $\alpha_1 = 0.44$ QP solution that have been projected back to the QP plane at different frequencies.*

functions in (1.5)-(1.6). In particular, using the numerical values of the amplitude-phase variables A_j and B_j, (1.11) gives the value of the leading-order scalar field contribution, $\phi_1(t, x)$. The $\mathcal{O}(\epsilon^2)$ contribution to the derivatives of metric functions come from

$$\partial_x \delta_2(t,x) = -\sin(x)\cos(x)\left((\partial_x\phi_1)^2 + (\partial_t\phi_1)^2\right) , \tag{1.24}$$

$$\partial_x A_2(t,x) = -\frac{1-d+\cos(2x)}{\sin(x)\cos(x)}(A_2 - 1) - \sin(x)\cos(x)\left((\partial_x\phi_1)^2 + (\partial_t\phi_1)^2\right) , \tag{1.25}$$

$$\text{with } A_2(t,x) = -\frac{\cos^d(x)}{\sin^{d-1}(x)}\int_0^x \tan^{d-1}(y)\left((\partial_t\phi_1)^2 + (\partial_x\phi_1)^2\right) dy\,. \tag{1.26}$$

The L^2-norm of the differences between (1.24)-(1.25) and (1.5)-(1.6) would constitute the residuals of the Einstein equations. However, while the leading-order contribution to the residuals is $\mathcal{O}(\epsilon^4)$, there are in fact higher order terms that enter into the calculation of $\partial_t\phi$. A careful evaluation of the constraints would therefore include calculating the $\mathcal{O}(\epsilon^4)$ term in the metric function $A(t, x)$ so that the product $A(\Phi^2 + \Pi^2)$ would include terms $\mathcal{O}(\epsilon^6)$. Instead, we limit our focus to examining only the difference between (1.5) and (1.24), which does not suffer from higher-order contributions. The examination of residuals is taken as a suggestion of how well a TTF solution continues to satisfy the Einstein equations throughout its evolution. In figure 1.6, we show the absolute and relative L^2-norms both QP and high temperature solutions.

1.5 Time Evolution of Quasi-Periodic Solutions

Using the numerical evolution methods from [**?**], we use a variety of quasi-periodic and high-temperature solutions discussed above as initial data. We then examine their evolution under

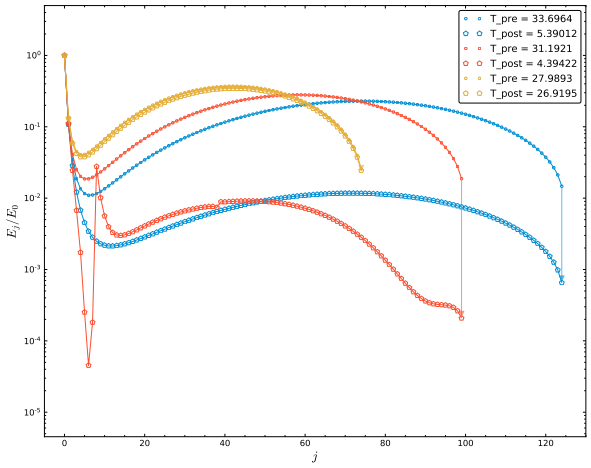

(a) *QP solutions perturbed to $T_{max} = 30.00$, which were then used as seeds for the nonlinear solver. Arrows are oriented from pre-optimized to post-optimized solutions.*

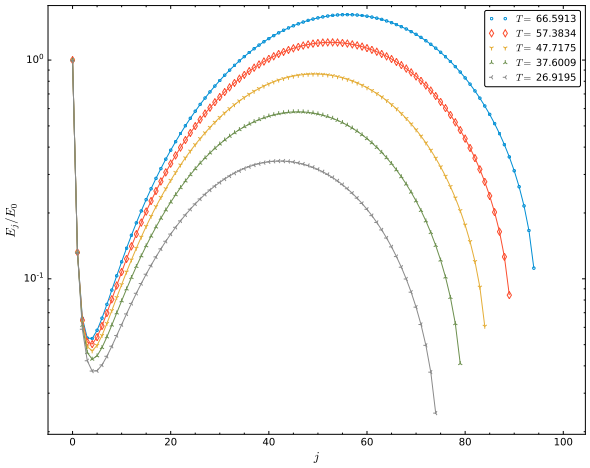

(b) *Extensions of the $j_{max} = 50$ solution from figure 1.4a to larger j_{max} solutions using tail fitting on only the final 5 modes of the solution.*

Figure 1.4: *Constructing high temperature solutions "by hand."*

(1.15)-(1.16).

For each type of solution below, we can generate the following plots:

- **Ricci scalar at the origin**
- **Einstein equation residuals**
- **Energy spectra (mode evolution, full spectrum evolution)**
- **QP equation residuals**
- **Projection of amp/phase intermediate solutions back to QP plane**

1.5.1 Quasi-Periodic Solutions

Consider first the evolution of a known QP solution. We see in figure 1.7 that the fraction of the total energy in the lowest-j modes remains constant over the duration of the evolution, while the fraction in the highest-j modes increases after $\tau \simeq 0.3$. Given the scale of the energy in the modes $j \geq 96$, this growth can mainly be attributed to numerical errors.

To better understand how well the QP solutions continue to satisfy the TTF equation throughout their time evolution, we evaluate the residuals of (1.19) using data taken during the evolution. Figure 1.8 is a sample of the L^2-norm of these residuals using values for the amplitude-phase variables $A_j(\tau)$, $B_j(\tau)$ during evolution. We also examine changes in the spectrum during the evolution, and show that there is very little deviation between the initial and final spectra for QP solutions beyond numerical drift.

Furthermore, we can attempt to project the evolved solutions back to the QP plane at various times

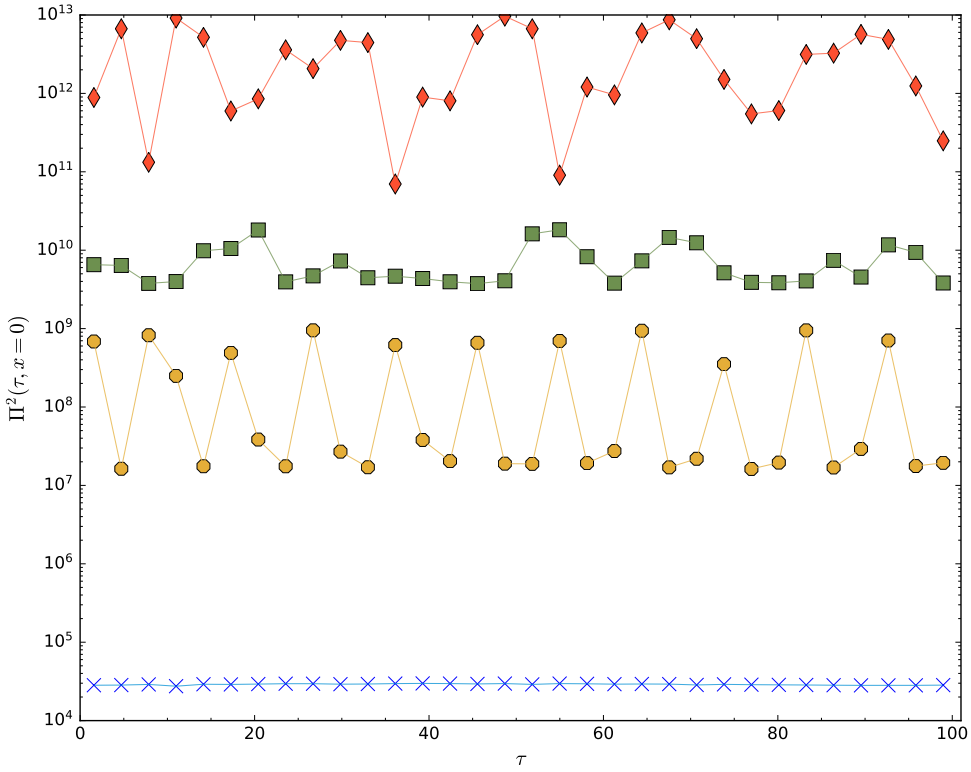

Figure 1.5: *Comparing the upper envelope of* Π^2 *at the origin per light-crossing time for selected low- and high-temperature solutions with* $\epsilon = 1$*:* $j_{max} = 375$*, QP* $T \simeq 3.15$ *(blue crosses);* $j_{max} = 75$*, high-temperature* $T \simeq 26.9$ *(yellow octagons);* $j_{max} = 100$*, high temperature* $T \simeq 75.35$ *(green squares);* $j_{max} = 95$*, high temperature* $T \simeq 66.6$ *(red diamonds).*

to explore if these solutions loose their quasi-periodic nature. We observe that the time-evolved, low-temperature QP solutions are easily projected back to the solution plane at all times during the evolution, and that the resulting solutions solve the QP equation (1.19) to a high degree of accuracy (see figure 1.9a). While this is to be expected for such low-temperature QP solutions, we will soon see that even padding a known QP solution with zeros causes the loss of quasi-periodicity during evolution. For comparison, figure 1.9b shows the results of attempting to project a QP solution that has been padded with zeros back to the QP plane during its evolution. Note the scale on the plot of the L^2-norm in either case.

Padded QP Solutions

In an effort to extend the space of QP solutions, another method used to find solutions that exist nearby known QP solutions – but are not accessible through perturbative or conventional seeding methods – is to pad a given quasi-periodic solution with extra modes that are initially set to zero. Upon amplitude-phase evolution, the energy in the lower-j modes will flow into the higher-j modes and a new quasi-periodic solution may be found. In figure 1.10, we construct initial data out of a known $j_{max} = 100$, $T \simeq 3.14$ solution by padding with zeros up to $j_{max} = 200$. As in the case of unpadded QP solution, the fraction of the total energy in the first four modes does not vary

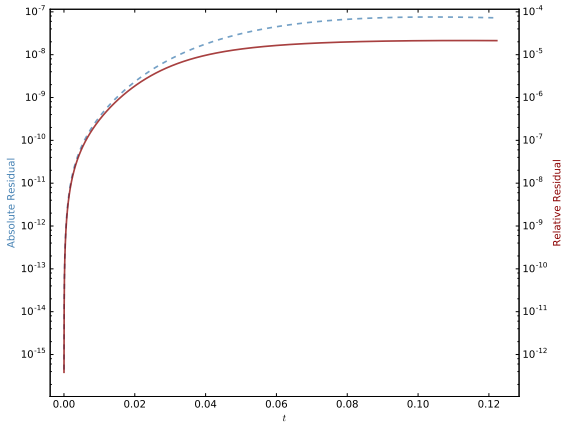

(a) *An* $\alpha_1 = 0.44$*,* $j_{max} = 100$ *QP solution with* $\epsilon = 0.001$*.*

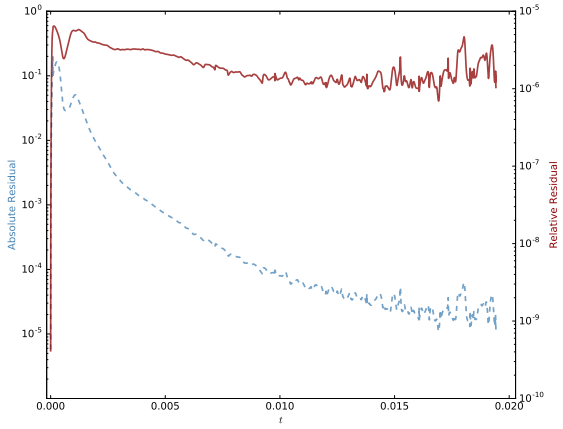

(b) *A* $j_{max} = 100$*, high-temperature solution is padded with zeros to* $j_{max} = 125$ *and evolved with* $\epsilon = 0.001$*.*

Figure 1.6: *Residuals from evaluating the constraints for QP and high temperature solutions.*

during the evolution and the highest modes accumulate some numerical error before levelling off. In figure 1.10d, we see the accumulation of numerical error in the higher modes as the evolution progresses. Also included is the value of the Ricci scalar at the origin, and the residuals of the QP equation throughout the evolution.

Despite the somewhat normal profile of the spectra of padded QP solution, we see in figure 1.9b that intermediate solutions during the evolution in fact *do not* project back to the QP plane. Rather, as hinted at by the Einstein equation residuals shown in figure 1.10f, the solutions have drifted away from their quasi-periodic initial data. It remains to be seen whether such profiles would be stable in the fully nonlinear system.

Using a known QP solution, we may ask how far away from the solution plane we can move by padding with an incremental number of zeros. In figure 1.11, we show the result of using intermediate solutions from the amplitude/phase evolution of a $j_{max} = 100$ QP solution padded with only five modes (initially set to zero). Despite QP solutions existing for $j_{max} = 105$, no solution was found when using the padded solution – at any point in its evolution – as a seed.

1.5.2 High-Temperature Solutions

High-temperature solutions are those that are found by repeated applications of energy perturbations described in § 1.4.2. These come in several varieties based on the methods used to obtain them; namely, the frequency of projection back to the QP solution plane versus constructing solutions "by hand." Note that solutions obtained without projecting back to the QP plane, or via the threshold temperature method, *are not* robust in the limit of large j_{max} (see Appendix C for further discussion on the extension of high-temperature solutions to large j_{max}). However, it will be useful nonetheless to contrast their behaviour with other high-temperature solutions.

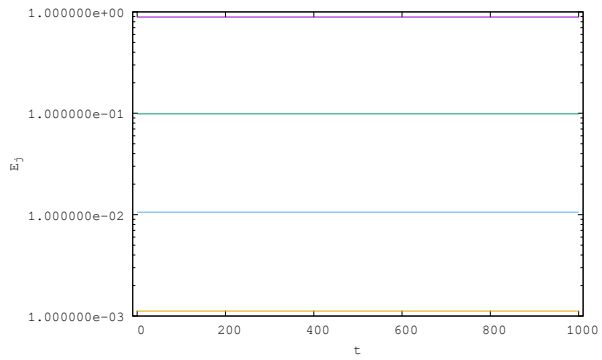

(a) *From top to bottom:* $j = 0, 1, 2, 3$ *(purple, green, blue, orange).*

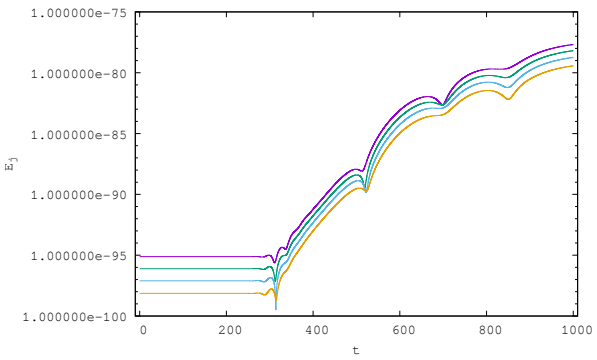

(b) *From top to bottom:* $j = 96, 97, 98, 99$ *(purple, green, blue, orange).*

Figure 1.7: *Amplitude-phase evolution of an* $\alpha_1 = 0.2$*,* $j_{max} = 100$*, QP solution with* $\epsilon = 0.01$*. Similar behaviour is observed for higher* j_{max} *solutions and over values of* $0.2 \leq \alpha_1 \leq 0.44$*.*

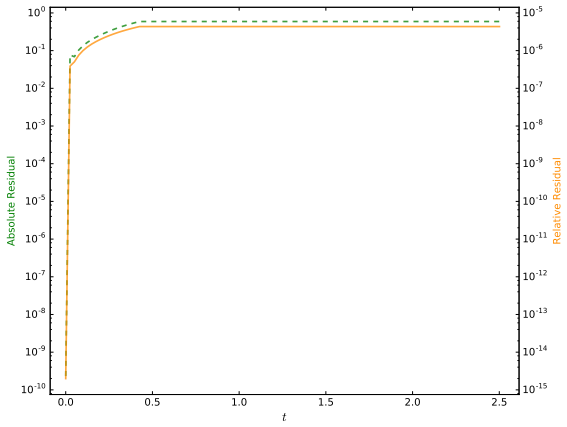

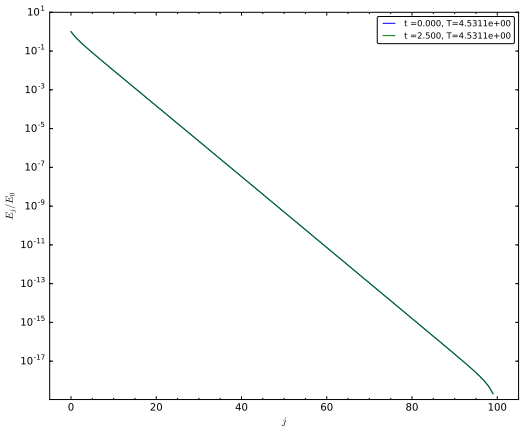

Figure 1.8: *Left:* L^2*-norm of the residuals of* (1.19) *evaluated at intervals of* 0.025 *during the evolution of a* $j_{max} = 100$*,* $\alpha_1 = 0.44$ *QP solution with* $\epsilon = 0.1$*. Right: The spectra of the QP solution at the beginning and end of the evolution.*

Regular Projections to the QP Plane

Here we examine a high-temperature solution obtained from repeatedly adding small amounts of energy to a $j_{max} = 100$, $\alpha_1 = 0.44$ QP solution. First, we consider threshold temperature solutions discussed in § 1.4.2 – those that are on the cusp of quasi-periodic data but cannot be found through solving (1.19) alone. See figure 1.12 for results.

Threshold temperature solutions behave much like low-temperature quasi-periodic solutions: no energy transfer occurs among the leading modes, while very little occurs in the highest modes. Note the scale in figure 1.12b. Unlike other QP solutions with similar total number of modes, the highest modes in threshold temperature solutions contain $\mathcal{O}(10^{-7})E_T$. This relatively high value of the fraction of the total energy means that numerical errors remain suppressed throughout the evolution.

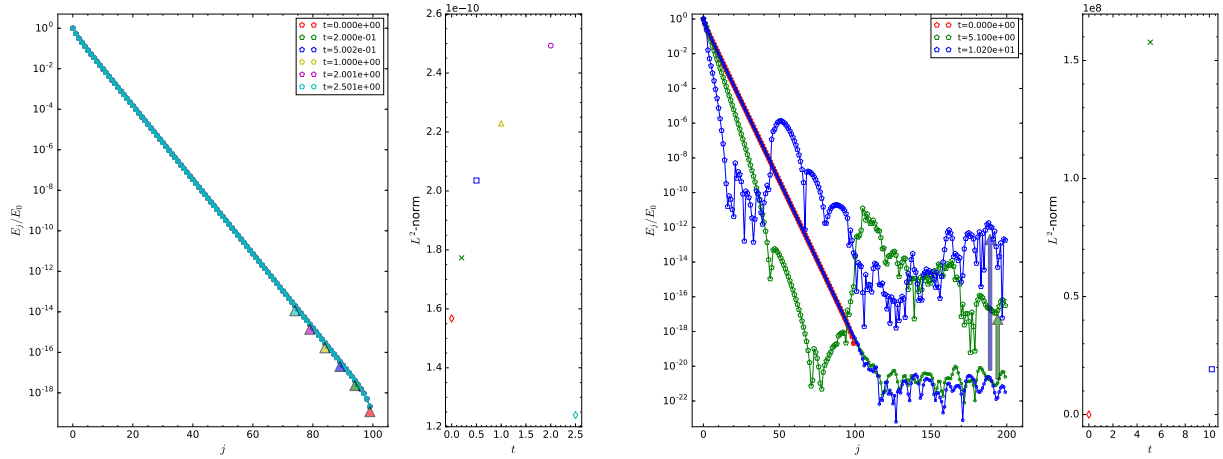

(a) *Projected solutions for a low-temperature, QP solution and their L^2-norms at $t \simeq 0.0, 0.2, 0.5, 1.0, 2.0, 2.5$ (red diamond, green cross, blue square, yellow triangle, magenta circle, blue diamond).*

(b) *The same QP solution is padded with zeros out to $j_{max} = 200$ and evolved in time. Intermediate solutions are projected back to the QP plane at $t \simeq 0.0, 5.1, 10.2, ...$ (red diamond, green cross, blue square ...)*

Figure 1.9: *Intermediate values from the amplitude/phase evolution of a solution are used as seeds for the nonlinear solver at various times. Arrows are oriented from amplitude/phase seed values (circles) to QP plane projections (pentagons).*

"By Hand" High-Temperature Solutions

Following the method outlined in § 1.4.3, we consider high-temperature solutions constructed by hand out of lower j_{max} solutions. We now examine the behaviour of one such solution under amplitude-phase evolution.

Attempt padding out to $j_{max} = 125$ and run the evolution: see figure 1.14

Finally, consider padding such a solution out to $j_{max} = 200$. See figure 1.15 for results.

The evolved profile of the high-temperature solution can no longer be projected back to the QP solution plane: figure 1.16.

Perturbing to an Intermediate Temperature Before Reoptimizing

Here, a QP solution is perturbed to a high temperature without regular projections back to the QP plane. At a pre-determined temperature cutoff, $T = 20.0$, the perturbation procedure is halted and the solution is used as a seed for the nonlinear solver. Instead of projecting to a QP solution at a high temperature, the nonlinear solver converges to a solution with only $T \sim 6.71$. We apply the amplitude-phase evolution procedure to the intermediate $T = 20.0$ solution in order to study how a solution for far away from the QP plane may behave. See figure 1.17 for results.

Padded Threshold Temperature Solutions

Padding the threshold temperature solution of $T \sim 5.4$ from $j_{max} = 100$ to $j_{max} = 200$ and then evolving in time produces very little change in the spectrum's profile. See figure 1.18 for results. Despite appearing to remain a high-temperature solution, the evolution of this profile renders it non-QP, as shown in figure 1.19. For a more concrete examination, figure 1.20 shows the threshold temperature solution for $j_{max} = 200$ as well as padded threshold solutions during their evolution. Under amplitude/phase evolution, the padded solution *does not* approach the known threshold solution.

1.6 Discussion

Acknowledgments The work of ND is supported in part by a Natural Sciences and Engineering Research Council of Canada PGS-D grant to ND, NSF Grant PHY-1606654 at Cornell University, and by a grant from the Sherman Fairchild Foundation. The work of BC and AF is supported by the Natural Sciences and Engineering Research Council of Canada Discovery Grant program. This research was enabled in part by support provided by WestGrid (www.westgrid.ca) and Compute Canada Calcul Canada (www.computecanada.ca).

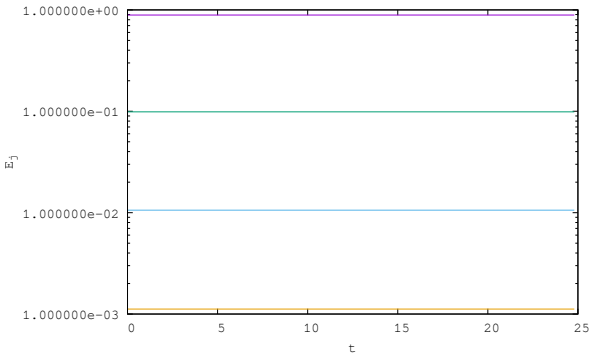

(a) *The evolution of the first four modes of the padded QP solution:* $j = 0, 1, 2, 3$ *(purple, green, blue, orange).*

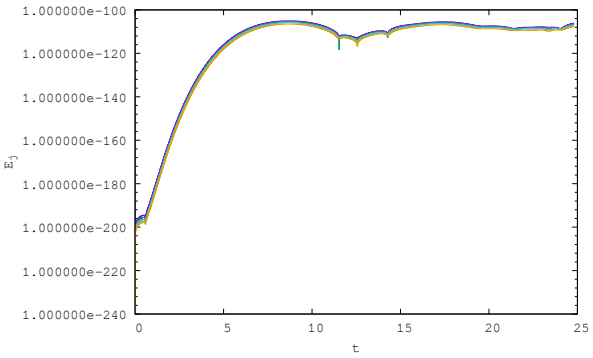

(b) *The evolution of the last four modes:* $j = 196, 197, 198, 199$ *(purple, green, blue, orange).*

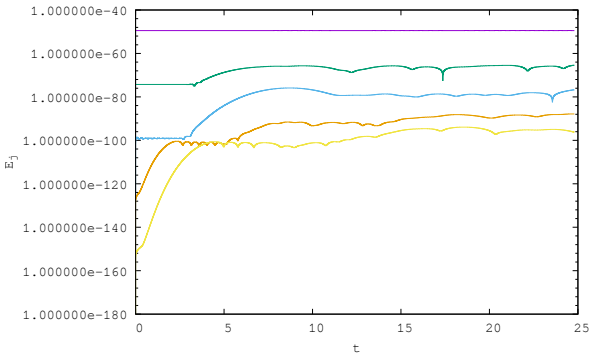

(c) *Comparing the evolution of a selection of modes:* $j = 50, 75, 100, 125, 150$ *(purple, green, blue, orange, yellow).*

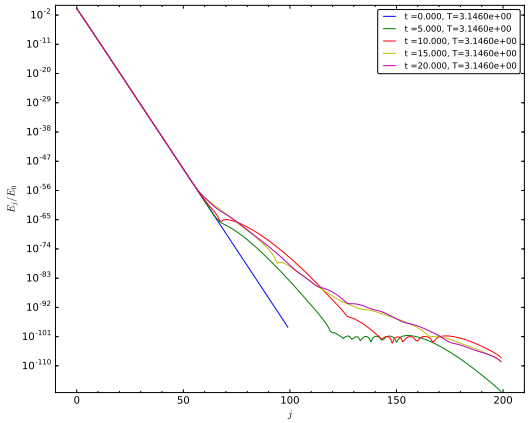

(d) *The total spectrum of the padded QP solution as a function of time.*

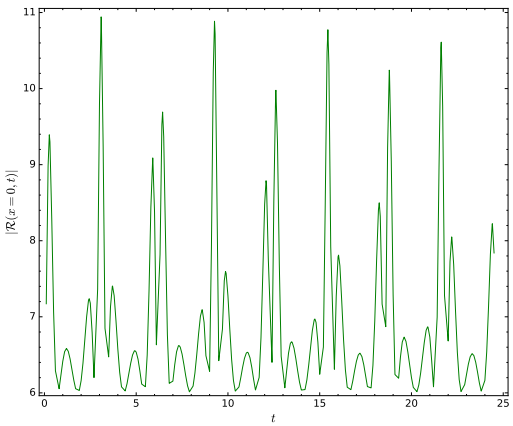

(e) *The Ricci scalar at the origin as a function of time for the padded QP solution.*

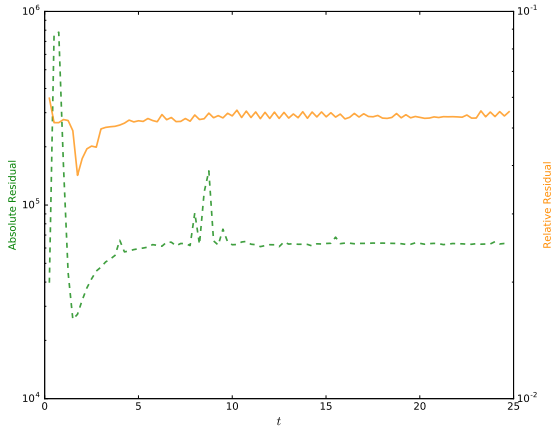

(f) *The residuals of the QP equation (1.19) throughout the amplitude-phase evolution of the padded QP solution.*

Figure 1.10: *The evolution of the padded QP solution for* $\alpha_1 = 0.2$ *and* $j_{max} = 200$*, with amplitude* $\epsilon = 0.1$*.*

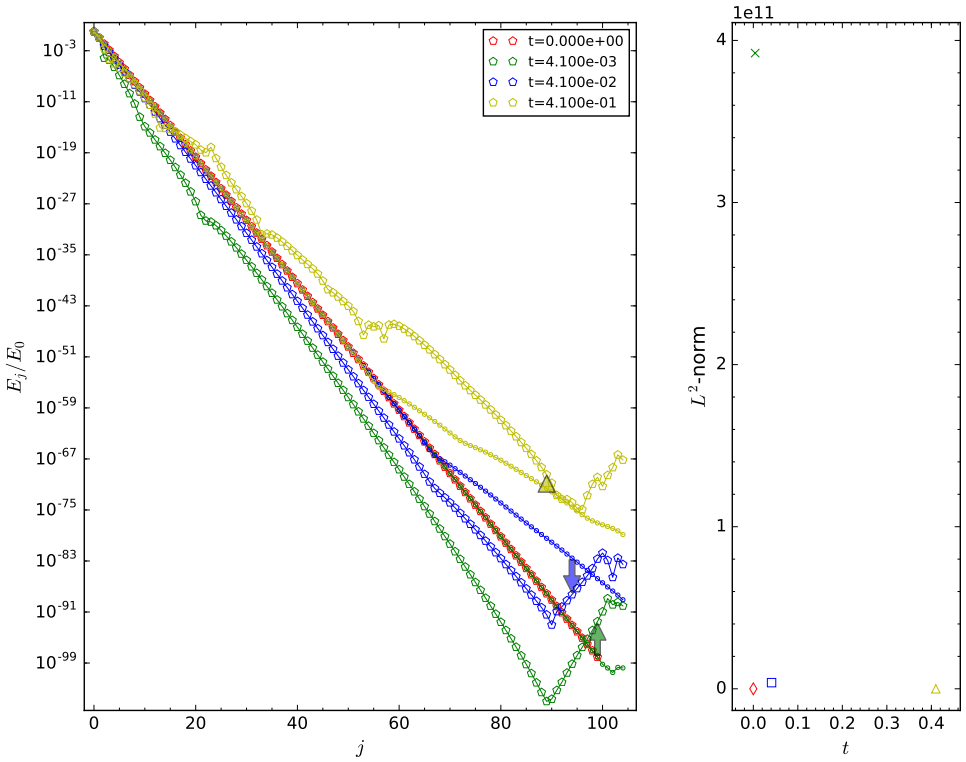

Figure 1.11: *Left: Normalized spectra for a $j_{max} = 100$, QP solution that has been padded with five extra modes, then evolved in time. Intermediate spectra are used as seeds for projecting back to the QP plane at times $\tau \simeq 4.1 \times 10^{-3}, 4.1 \times 10^{-2}, 4.1 \times 10^{-1}$ (green, blue, yellow). Arrows are oriented from seed spectra to best fit spectra. Right: Corresponding L^2-norms of the error for each solution.*

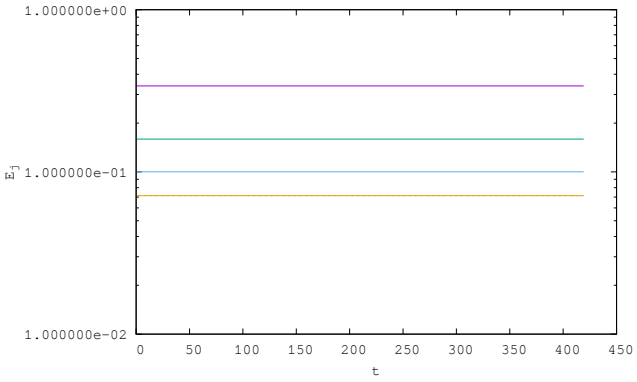

(a) $j = 0, 1, 2, 3$ *(purple, green, blue, orange).*

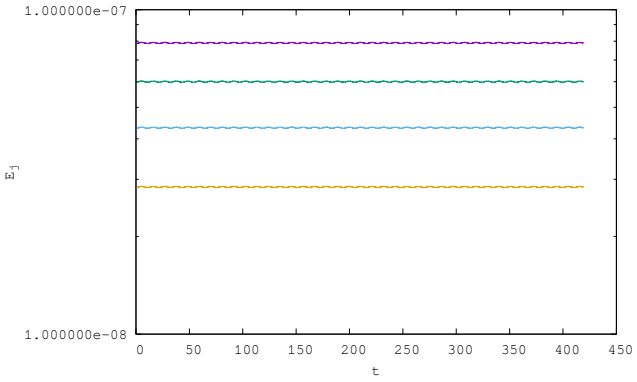

(b) $j = 96, 97, 98, 99$ *(purple, green, blue, orange).*

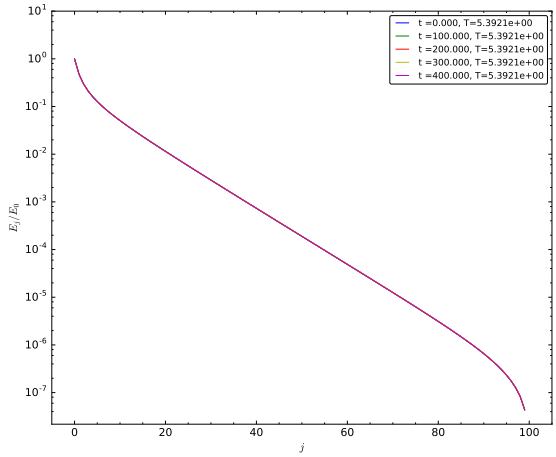

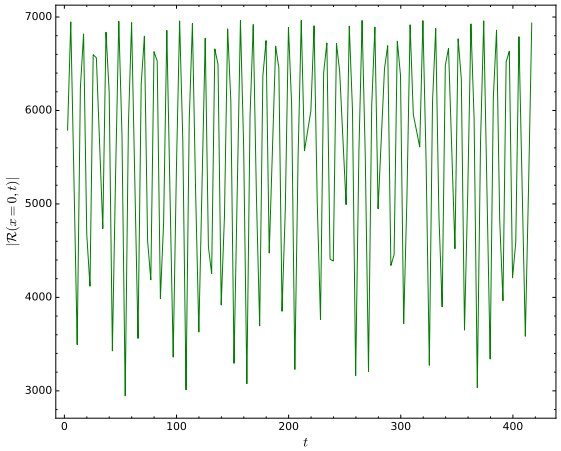

Figure 1.12: *Above: The evolution the fraction of the total energy in specific modes for a* $T \sim 5.4$*, threshold temperature solution for* $\tau \in [0, 4.25]$*. Below: Snapshots of the full spectrum at various times in its evolution, as well as the upper envelope of* $|\mathcal{R}(t, x = 0)|$ *when* $\epsilon = 0.1$*.*

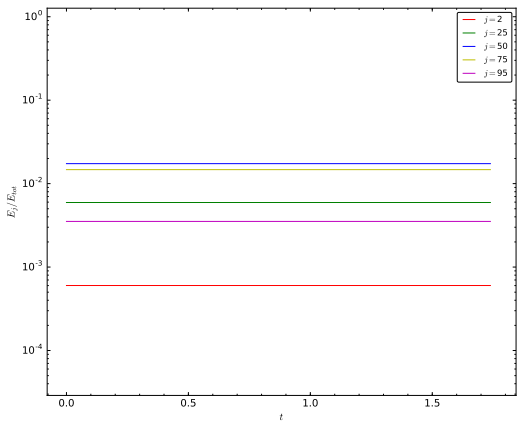

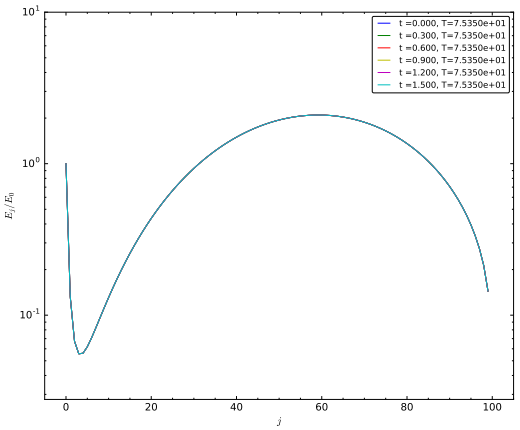

Figure 1.13: *The evolution of a high-temperature solution created by hand from lower* j_{max} *solutions.*

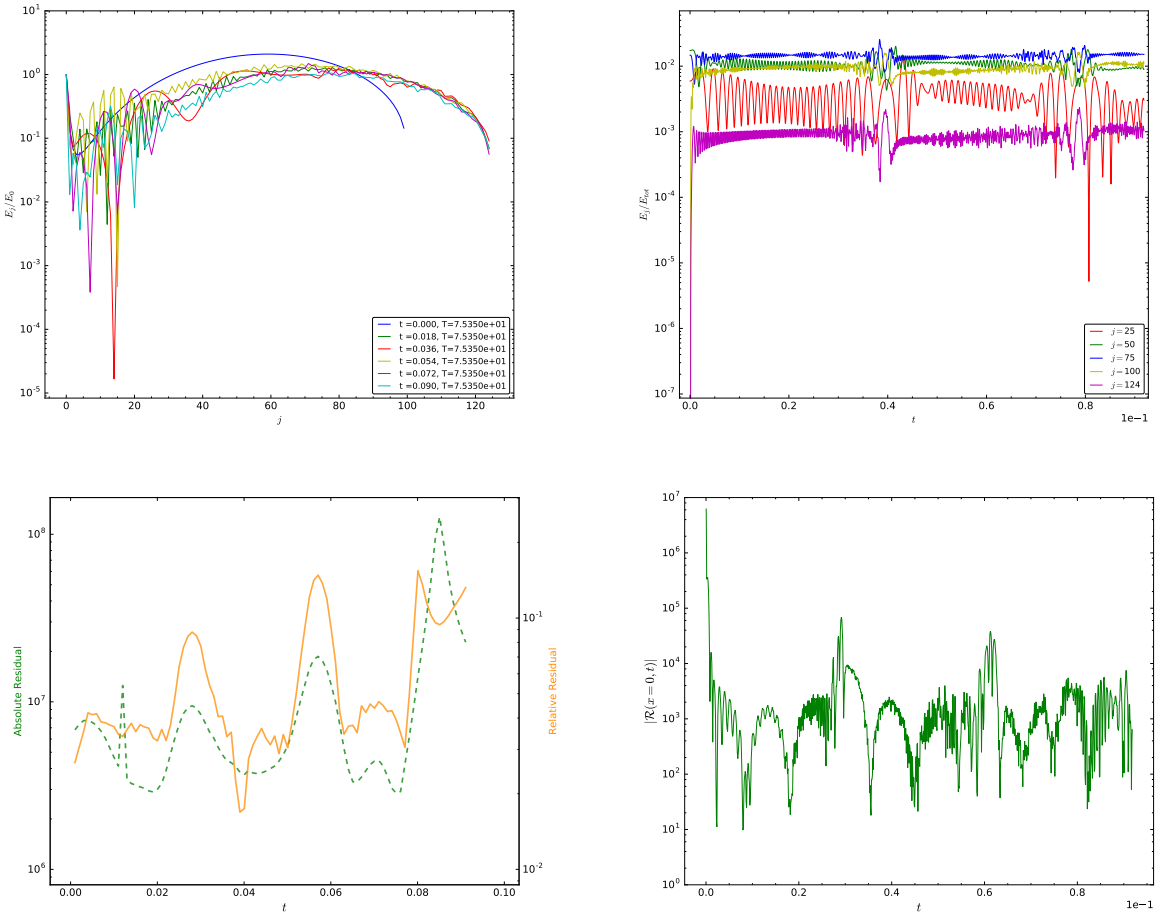

Figure 1.14: *Padding the same initial solution from figure 1.4, but with only* 25 *extra modes.*

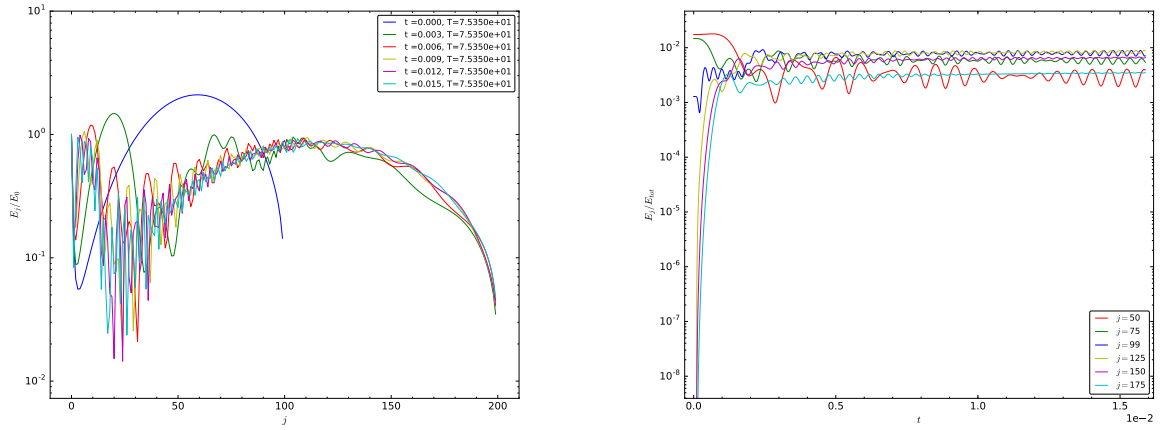

Figure 1.15: *Padding a* $j_{max} = 100$*, high temperature solution to* $j_{max} = 200$ *and evolving in time.* $\epsilon = 0.1$

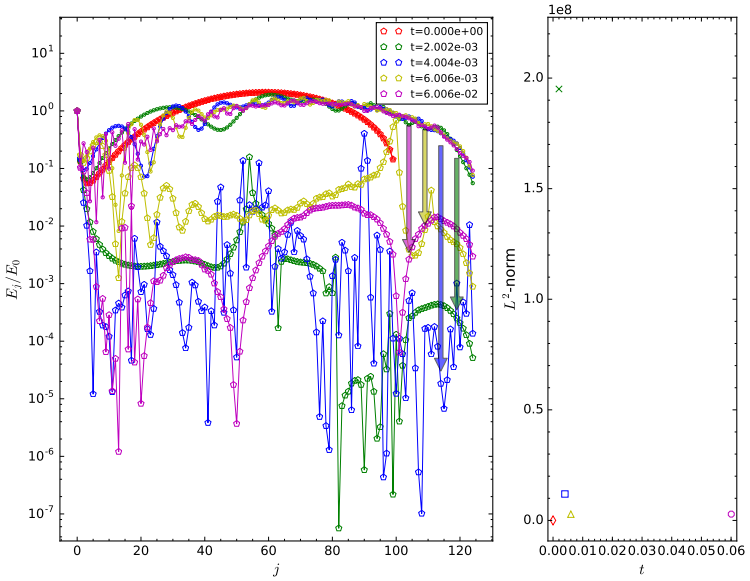

Figure 1.16: *A high-temperature solution is padded with* 25 *extra modes, then evolved in time. Above are the results of projecting back to the QP plane at* $t \simeq 0.002, 0.004, 0.006, 0.06$ *(red diamond, green cross, blue square, yellow triangle, magenta cirlce).*

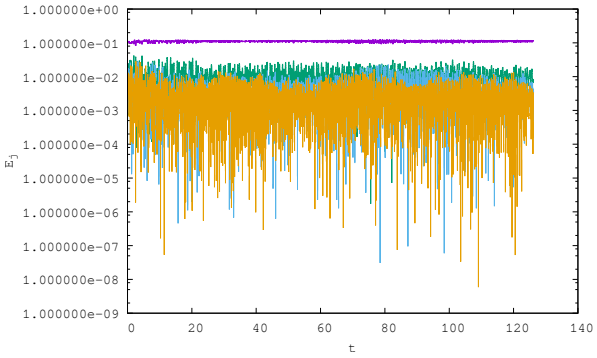

(a) *Evolution of the first four modes.*

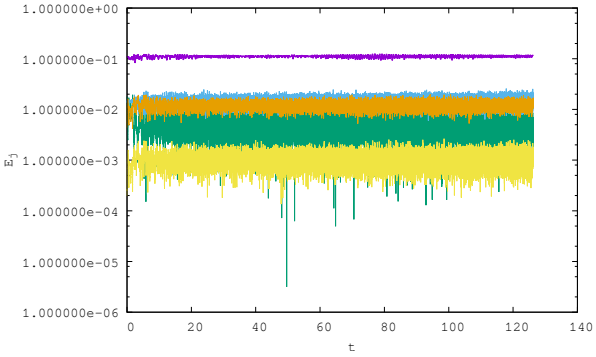

(b) *Comparative evolution of modes* $j = 0, 25, 50, 75, 99$.

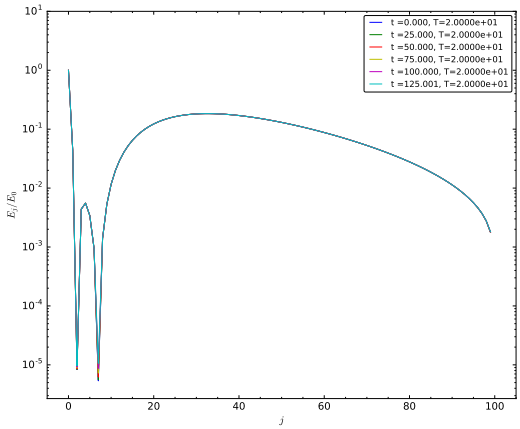

(c) *Energy spectrum at selected times throughout the evolution.*

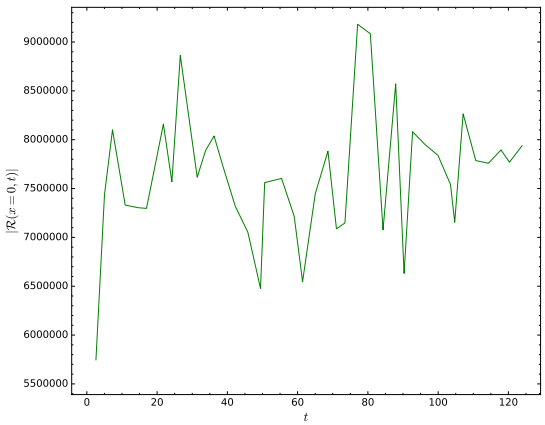

(d) *The upper envelope of the Ricci scalar at the origin, per light-crossing time.*

Figure 1.17: *The evolution of an intermediate, high-temperature solution that* does not *correspond to a solution of the QP equations.*

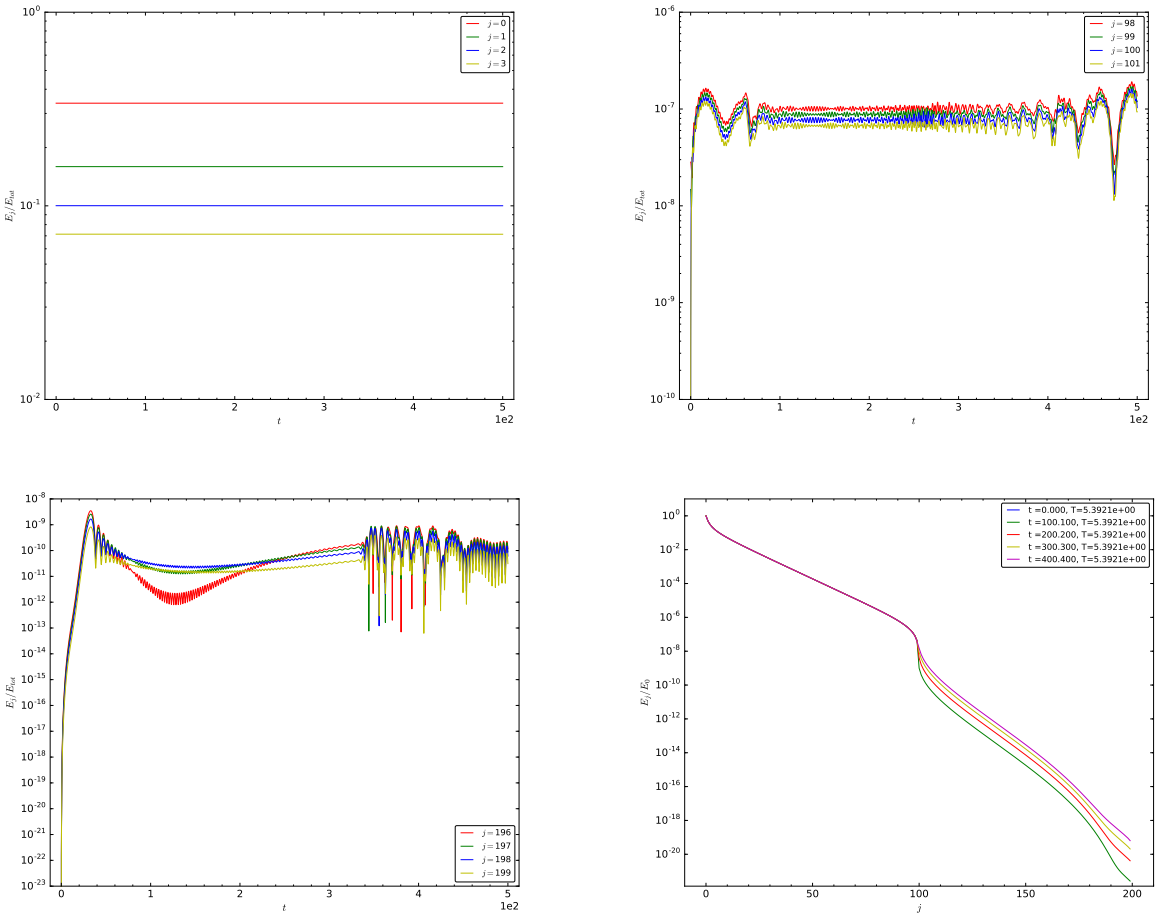

Figure 1.18: *Padding a threshold temperature solution*

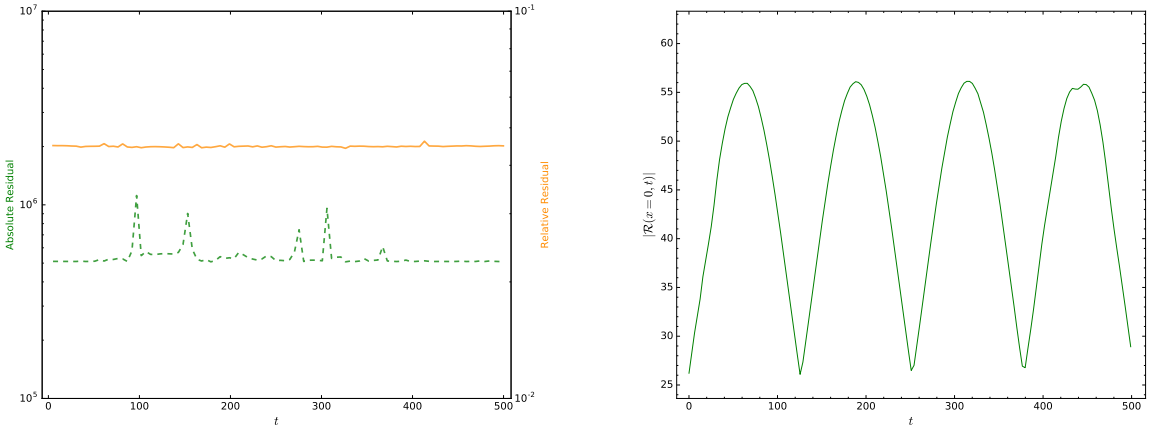

(a) *The residuals of* (1.19) *during the evolution of the padded threshold temperature solutions shown in figure 1.18.*

(b) *The upper envelope of the Ricci scalar at the origin per light-crossing time for the padded threshold temperature solution.*

Figure 1.19: *Despite the spectrum of the padded threshold temperature solution (figure 1.18) resembling that of lower-temperature QP solutions, these solutions move away from the QP plane and can no longer be projected back.*

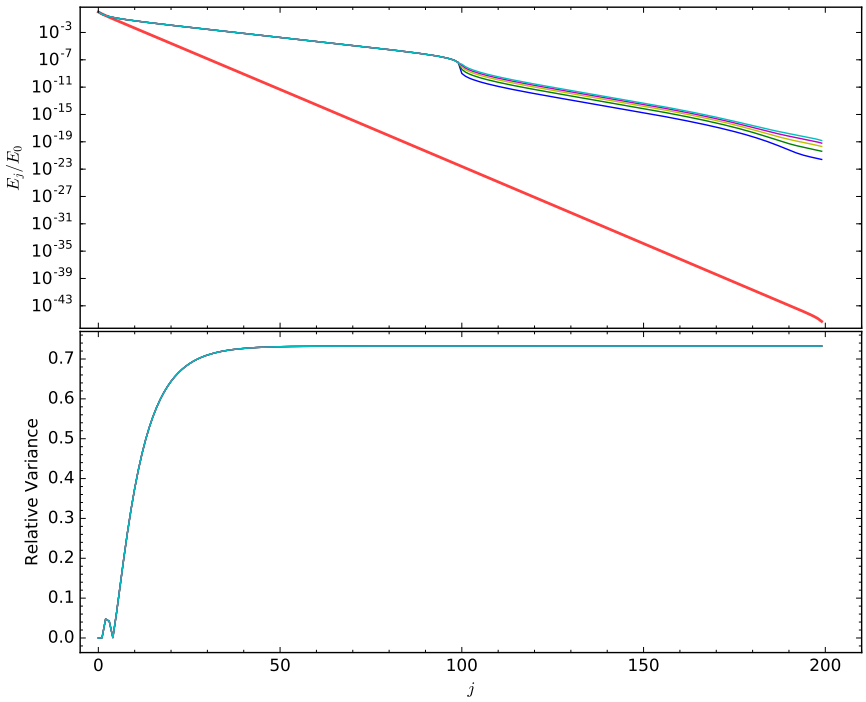

Figure 1.20: *Top: Overlay of the known threshold temperature solution for* $j_{max} = 200$ *(thick red line) with snapshots of the spectra of a* $j_{max} = 100$ *threshold solution that has been padded with zeros to* $j_{max} = 200$ *after amplitude/phase evolutions of* $\tau = 1, 2, 3, 4, 5 \times 10^{-5}$ *(blue, green, yellow, magenta, cyan). Bottom: The absolute value of the difference between the cumulative sums of the* $j_{max} = 200$ *threshold temperature solution and each snapshot spectrum (same colouring).*

Appendix

1.A Seeding Methods For Non-Linear Solvers

While it was originally proposed by [**?**] that the appropriate seed value for nonlinear solvers be given by the exponential relation ($j > 1$)

$$\alpha_j \sim \frac{3e^{-\mu j}}{2j+3} \tag{1.27}$$

in AdS_4, where $\mu = \ln(3/5\alpha_1)$, as j_{max} increased, the seed values diverged significantly from the true solutions (see figure 21 for a comparison between known QP solutions and the seeds generated by (.27)). Although this profile was sufficient for low j_{max} solutions, above $j_{max} \gtrsim 150$, (.27) no longer provided an adequate starting guess. To overcome this problem, exponential fitting was applied to the tail values of a known QP solution with lower j_{max}. Using this exponential fit, the data was extrapolated to a higher j_{max}.

Care was taken to avoid edge effects due to truncation when choosing the points that constituted the tail of the data. To illustrate the variance of the solution with truncation, we examine a fixed α_j value over a variety of j_{max}, starting with $\alpha_j = \alpha_{j_{max}}$. In table 2 we see that the value of α_{50} for QP solutions with $\alpha_1 = 0.2$ becomes impervious to truncation effects once $j_{max} > 55$.

To err on the side of caution, the modes $[j_{max} - 30,\ j_{max} - 10]$ were used from each QP solution to provide more accurate seed values for $j_{max} + 25$ solutions. See figure 22a for a comparison of seed values generated by tail fitting to actual QP solutions. The solutions found using this method of seeding versus those found from the seeding given in (.27) had relative differences on the order of 10^{-14} (see figure 22b).

1.B Auxiliary Integrals For Calculating the T, R, S Coefficients

The auxiliary coefficients X, Y, W, W^*, A, and V allow the symmetries of the T, R and S coefficients to be more easily recognized and therefore reduce the number of total calculations involved in determining (.34) - (.36). These auxiliary coefficients are written simply in terms of the eigenfunctions

j_{max}	α_{50}
50	1.74597252e-26
51	1.82668391e-26
52	1.83346256e-26
53	1.83408260e-26
54	1.83414138e-26
55	1.83414706e-26
60	1.83414768e-26
65	1.83414768e-26
70	1.83414768e-26
75	1.83414768e-26

Table 1.A.1: *α_{50} values for various j_{max} QP solutions.*

in (1.9) and their derivatives. Explicitly, they are

$$X_{ijkl} = \int_0^{\pi/2} dx\, e_i'(x)e_j(x)e_k(x)e_l(x)\sin(x)\cos(x)\left(\tan(x)\right)^{d-1} \tag{1.28}$$

$$Y_{ijkl} = \int_0^{\pi/2} dx\, e_i'(x)e_j(x)e_k'(x)e_l'(x)\sin(x)\cos(x)\left(\tan(x)\right)^{d-1} \tag{1.29}$$

$$W_{ijkl} = \int_0^{\pi/2} dx\, e_i(x)e_j(x)\sin(x)\cos(x)\int_0^x dy\, e_k(y)e_l(y)\left(\tan(y)\right)^{d-1} \tag{1.30}$$

$$W^*_{ijkl} = \int_0^{\pi/2} dx\, e_i'(x)e_j'(x)\sin(x)\cos(x)\int_0^x dy\, e_k(y)e_l(y)\left(\tan(y)\right)^{d-1} \tag{1.31}$$

$$A_{ij} = \int_0^{\pi/2} dx\, e_i'(x)e_j'(x)\sin(x)\cos(x) \tag{1.32}$$

$$V_{ij} = \int_0^{\pi/2} dx\, e_i(x)e_j(x)\sin(x)\cos(x)\,. \tag{1.33}$$

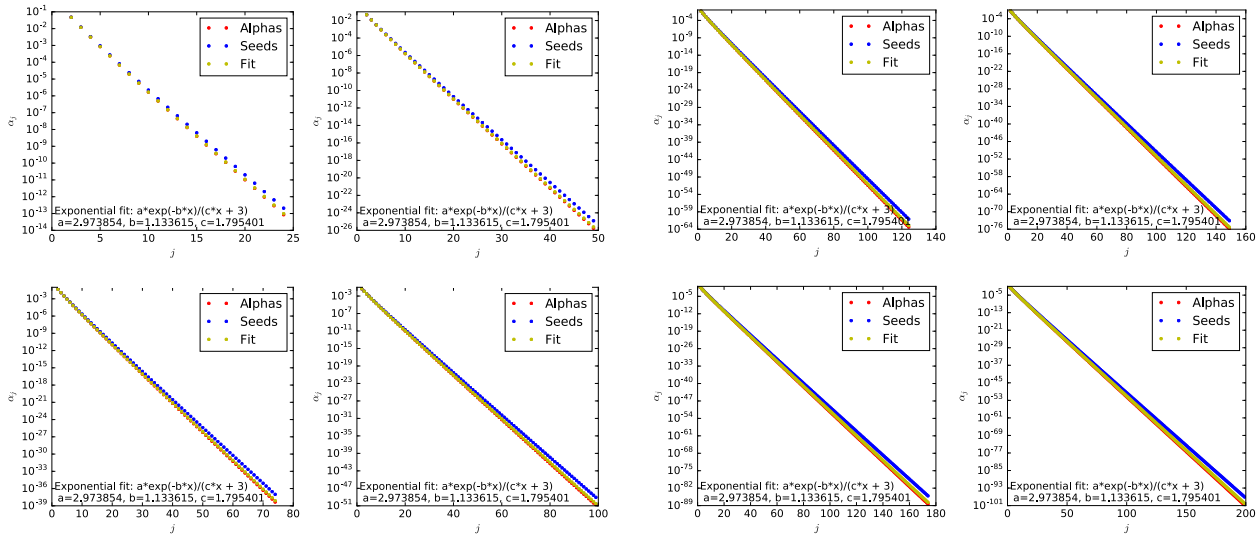

(a) $\alpha_1 = 0.2$ *QP solutions for* $j_{max} \in [25, 100]$. **(b)** $\alpha_1 = 0.2$ *QP solutions for* $j_{max} \in [140, 200]$.

Figure 1.A.1: *A comparison of seeds predicted by* (.27) *to known QP solution. Also included for comparison are the results of fitting the QP solutions to a generic exponential fit.*

In terms of these coefficients, the TTF source terms are given by

$$T_l = \frac{1}{2}\omega_l^2 X_{llll} + \frac{3}{2}Y_{llll} + 2\omega_l^4 W_{llll} + 2\omega_l^2 W^*_{llll} - \omega_l^2(A_{ll} + \omega_l^2 V_{ll}) \tag{1.34}$$

$$\begin{aligned} R_{il} = {} & \frac{1}{2}\left(\frac{\omega_i^2 + \omega_l^2}{\omega_l^2 - \omega_i^2}\right)(\omega_l^2 X_{illi} - \omega_i^2 X_{liil}) + 2\left(\frac{\omega_l^2 Y_{ilil} - \omega_i^2 Y_{lili}}{\omega_l^2 - \omega_i^2}\right) \\ & + \left(\frac{\omega_i^2\omega_l^2}{\omega_l^2 - \omega_i^2}\right)(X_{illi} - X_{lili}) + \frac{1}{2}(Y_{iill} + Y_{llii}) + \omega_i^2\omega_l^2(W_{llii} + W_{iill}) \\ & + \omega_i^2 W^*_{llii} + \omega_l^2 W^*_{iill} - \omega_l^2(A_{ii} + \omega_i^2 V_{ii}) \end{aligned} \tag{1.35}$$

$$\begin{aligned} S_{ijkl} = {} & -\frac{1}{4}\left(\frac{1}{\omega_i + \omega_j} + \frac{1}{\omega_i - \omega_k} + \frac{1}{\omega_j - \omega_k}\right)(\omega_i\omega_j\omega_k X_{lijk} - \omega_l Y_{iljk}) \\ & - \frac{1}{4}\left(\frac{1}{\omega_i + \omega_j} + \frac{1}{\omega_i - \omega_k} - \frac{1}{\omega_j - \omega_k}\right)(\omega_j\omega_k\omega_l X_{ijkl} - \omega_i Y_{jikl}) \\ & - \frac{1}{4}\left(\frac{1}{\omega_i + \omega_j} - \frac{1}{\omega_i - \omega_k} + \frac{1}{\omega_j - \omega_k}\right)(\omega_i\omega_k\omega_l X_{jikl} - \omega_j Y_{ijkl}) \\ & - \frac{1}{4}\left(\frac{1}{\omega_i + \omega_j} - \frac{1}{\omega_i - \omega_k} - \frac{1}{\omega_j - \omega_k}\right)(\omega_i\omega_j\omega_l X_{kijl} - \omega_k Y_{ikjl})\,. \end{aligned} \tag{1.36}$$

1.C Frequency of Solution Checking

The frequency of applying the nonlinear solver to project back down to the QP solution plane is an important part of ensuring that the perturbative method remains applicable. If QP solutions are perturbed by too large an energy, or for too many iterations, the intermediate solutions may not be

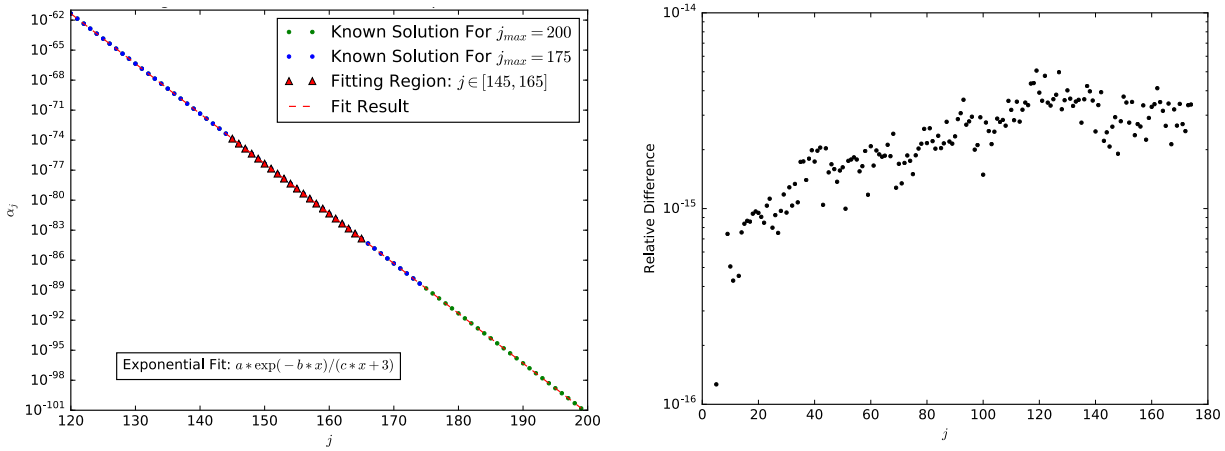

(a) *Fitting the tail of the $j_{max} = 175$ spectrum to construct a seed for $j_{max} = 200$ at fixed $\alpha_1 = 0.2$. Also included is actual QP spectrum for $j_{max} = 200$.*

(b) *Relative difference between $\alpha_1 = 0.2$ QP solutions found using tail-fitting and those from the exponential profile (.27).*

Figure 1.A.2: *The process and result of tail fitting the α_j spectra of QP solutions to generate better seed values.*

close enough to the solution plane to provide an adequate seed value. Such was the concern when examining the purported high-temperature solutions from existing sources.

For example, consider the process of applying perturbations of $\delta E = 0.01\%$ up to some intermediate temperature without projecting back to the QP plane, then projecting back every 100 iterations until a maximum temperature is reached. Starting with the QP solution corresponding to $\alpha_1 = 0.2$, the lower panel of figure 23 shows the result of repeated perturbations of $\delta E = 0.01\%$ that are not projected back the to QP plane.

The behaviour of the spectra differ for the low and high j_{max} cases. For the $j_{max} = 50$ solutions, the spectra in the lower panel of the figure can be remain smooth through more than 27,000 iterations of δE perturbations. When a temperature of approximately 17 is reached, the spectrum is used as a seed value for the nonlinear solver and a smooth solution is found. Continuing with the same δE, but reapplying the nonlinear solver produces mixed results; the temperatures of increasing iterations do not increase monotonically, but do always project back to a solution with nearly the same temperature. However, the spectra themselves develop kinks by iteration 3,100 that are indicative of a change of sign in the alpha values and a breakdown of the perturbative condition. Because only a small number of modes are considered, numerical solutions are still found by the Newton-Raphson solver but no longer represent physical states. Continuing this procedure, we find that the solver fails to find a solution even at the modest temperature of $T \simeq 38$.

The behaviour of the $j_{max} = 150$ solutions is consistent with their lower-mode number counterparts, albeit more pronounced. We see that kinks in the spectrum develop even when the nonlinear solver has not been applied. The intermediate solution used as a seed for the nonlinear solver did not project back to a nearby temperature, instead falling from $T \simeq 14.2$ to $T \simeq 4.3$. As the perturbative procedure continued, projection back to the QP plane was only possible in for a short time before no solution could be found. Note the numerous spikes in the energy spectrum shown in the upper

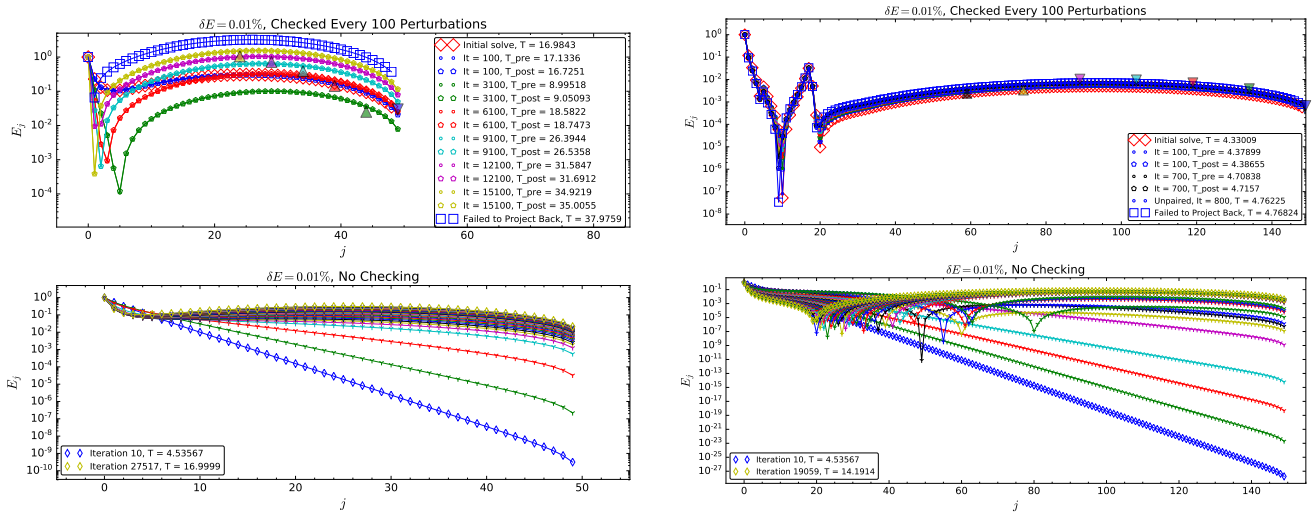

Figure 1.C.1: *Left: the result of unchecked perturbations of a $j_{max} = 50$ QP solution up to an intermediate temperature before switching to regular checking. Right: the same procedure is applied to a $j_{max} = 150$ QP solution.*

panel. For $j_{max} = 150$, we conclude that no physically relevant high-temperature solutions exist, even as low as $T \simeq 4.76$.